Solid-state NMR evidence for an antibody-dependent conformation of the V3 loop of HIV-1 gp120

David P. Weliky[1,2], Andrew E. Bennett[2], Anat Zvi[3], Jacob Anglister[3], Peter J. Steinbach[4] and Robert Tycko[2]

[1]Department of Chemistry, Michigan State University, East Lansing, Michigan 48824, USA. [2]Laboratory of Chemical Physics, National Institute of Diabetes and Digestive and Kidney Diseases, National Institutes of Health, Bethesda, Maryland 20892-0520, USA. [3]Department of Structural Biology, The Weizmann Institute of Science, Rehovot 76100, Israel. [4]Center for Molecular Modeling, Center for Information Technology, National Institutes of Health, Bethesda, Maryland 20892-5626, USA.

Solid-state NMR measurements have been carried out on frozen solutions of the complex of a 24-residue peptide derived from the third variable (V3) loop of the HIV-1 envelope glycoprotein gp120 bound to the Fab fragment of an anti-gp120 antibody. The measurements place strong constraints on the conformation of the conserved central GPGR motif of the V3 loop in the antibody-bound state. In combination with earlier crystal structures of V3 peptide–antibody complexes and existing data on the cross-reactivity of the antibodies, the solid-state NMR measurements suggest that the Gly-Pro-Gly-Arg (GPGR) motif adopts an antibody-dependent conformation in the bound state and may be conformationally heterogeneous in unbound, full-length gp120. These measurements are the first application of solid-state NMR methods in a structural study of a peptide–protein complex.

The third variable (V3) loop region of the HIV-1 envelope glycoprotein gp120 plays a significant role in HIV infection and AIDS. As the principal neutralizing determinant of the virus[1], the V3 loop elicits potently neutralizing antibodies[2,3] and has been a target for AIDS vaccine development[4]. The V3 loop is also required for viral entry into target T cells and macrophages[5], interacts with chemokine co-receptors on the surfaces of these cells[6–9] and is a determinant of viral tropism[6,10]. The highly variable amino acid sequence of the V3 loop contributes to the ability of HIV to escape the host immune response, but it contains a highly conserved[11] central Gly-Pro-Gly-Arg (GPGR) motif that has been proposed to have structural and biological significance[5,11,12]. The GPGR motif has been predicted to adopt a type II β-turn conformation[11,13]. Crystal structures of V3 peptides bound to Fab fragments of neutralizing monoclonal antibodies[12,14,15], in which the peptides derive from gp120 of HIV-1 strain MN and the antibodies were elicited with a disulfide-linked peptide representing the entire V3 loop of strain MN, have revealed a more complex, double β-turn conformation. A similar GPGR conformation has been obtained from liquid-state NMR measurements on a bacteriophage coat protein–V3 peptide fusion protein solubilized in micelles[16]. NMR studies of unbound V3 peptides in solution indicate fractional population of type I and/or type II β-turns by the GPGR motif[17–22]. To promote crystallization, the V3 loop was deleted from the gp120 construct in a recent crystal structure of a ternary CD4–gp120–antibody Fab complex[23]. Significant questions remain[12,15] regarding the uniqueness of the GPGR conformation in gp120–antibody and gp120–chemokine receptor complexes, as well as in unbound gp120.

In this letter, we report a structural study of the V3 loop peptide RP135[1,24], which comprises the central 24 residues of the 40-residue V3 loop of HIV-1 strain IIIB (residues 308–331, sequence Asn-Asn-Thr-Arg-Lys-Ser-Ile-Arg-Ile-Gln-Arg-Gly-Pro-Gly-Arg-Ala-Phe-Val-Thr-Ile-Gly-Lys-Ile-Gly), bound to the neutralizing monoclonal anti-gp120 antibody 0.5β (ref. 2), which was elicited with full-length gp120 of strain IIIB ($gp120_{IIIB}$). We apply two recently developed ^{13}C solid-state NMR techniques[25–28] to frozen solutions of the peptide–antibody Fab complex in which the peptide is doubly ^{13}C-labeled. The solid-state NMR measurements provide information about the peptide backbone conformation in the GPGR motif. We find that the GPGR conformation in the RP135–0.5β complex differs significantly from the previously reported and predicted GPGR conformations. Our results indicate that the conformation in V3 loop–antibody complexes is antibody dependent and suggest that the GPGR motif may be conformationally heterogeneous in unbound gp120. This work also demonstrates the capability of the solid-state NMR methods to provide atomic-level local structural information in high-molecular-weight, noncrystalline systems.

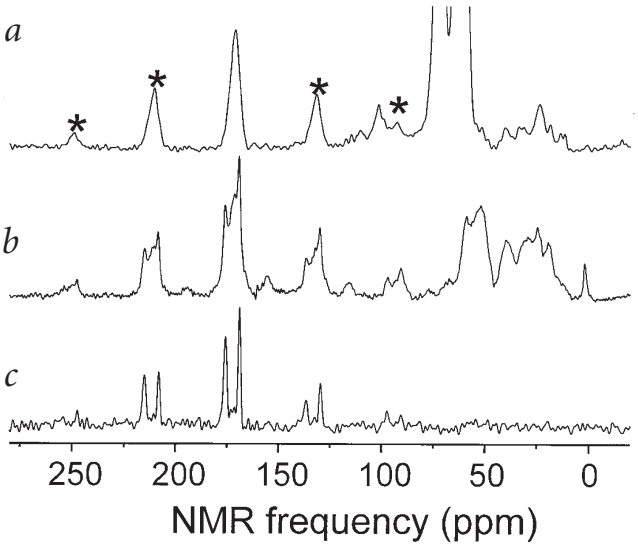

Fig. 1 ^{13}C-NMR spectra of the gp120 V3 loop peptide RP135, with ^{13}C labels at the carbonyl sites of Pro 320 and Gly 321 (sample 2). ***a,*** The free peptide in frozen solution (1:1 v/v glycerol/H_2O, pH 7.2, -125 °C). Glycerol was added to suppress crystallization. ***b***, ***c***, The complex of the peptide with Fab fragments of the anti-gp120 monoclonal antibody 0.5β (pH 7.0, no glycerol, -125 °C, 4 mM peptide and Fab concentrations). All spectra were acquired at a carrier frequency of 100.4 MHz, with magic-angle spinning at ν_R = 3.94 kHz. The frequency scale indicates chemical shifts relative to tetramethylsilane, giving isotropic shifts near 175 p.p.m. for carbonyl carbons. Asterisks indicate spinning sideband lines, which are separated from the isotropic shifts by integral multiples of ν_R. Large signals between 55 and 80 p.p.m. in (*a*) from natural-abundance ^{13}C in glycerol have been cropped. In (*b*), large natural-abundance ^{13}C-NMR signals, primarily from the Fab, appear in both the carbonyl and the aliphatic regions of the spectrum. In (*c*), natural-abundance signals are suppressed by double-quantum filtering, resulting in a clean spectrum of the labeled carbonyl sites of the antibody-bound peptide. This spectrum corresponds to the data point at 8.12 ms in Fig. 2*b*.

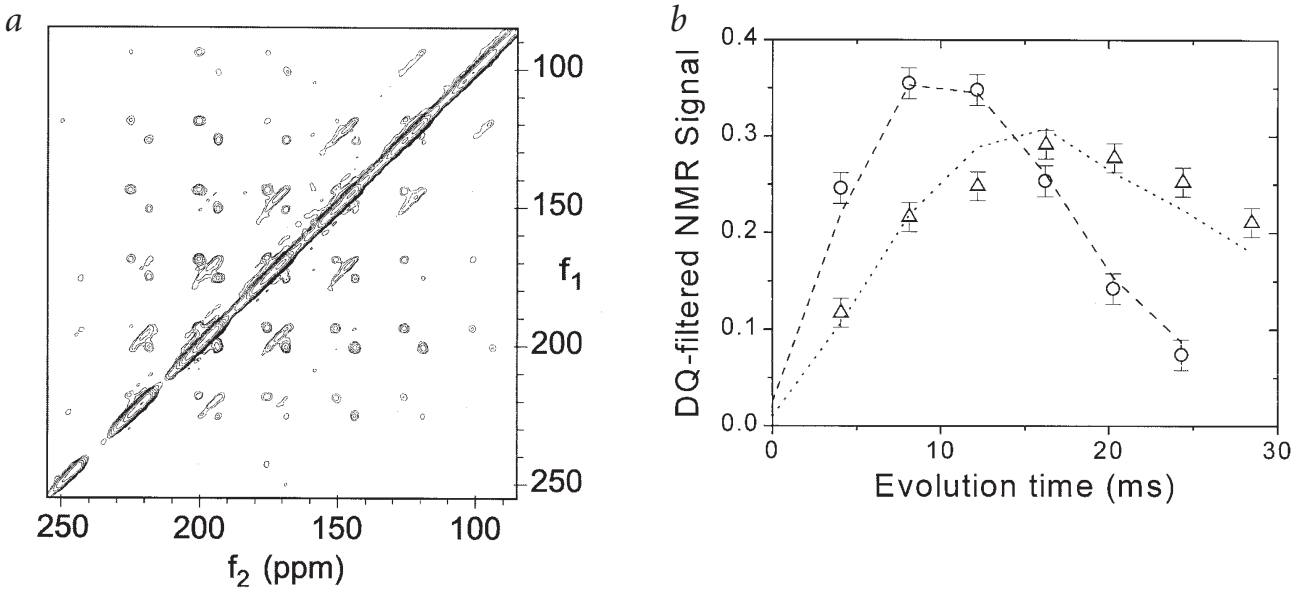

Fig. 2 Examples of structural data from solid-state NMR measurements on the RP135–0.5β Fab complex in frozen solution. ***a***, A 2D MAS exchange spectrum of the complex with ^{13}C labels at carbonyl sites of Pro 320 and Gly 321 of RP135 (sample 2), at ν_R = 2.5 kHz. Intersite crosspeaks, which connect spinning sideband lines of the two labeled carbonyl sites and appear as doublets oriented perpendicular to the diagonal of the 2D spectrum, contain the structural information. ***b***, Experimental CTDQFD data for sample 2 (circles) and sample 3 (triangles), at ν_R = 3.94 kHz. Sample 3 contains the complex with ^{13}C labels at Gly 321 and Arg 322 of RP135. CTDQFD simulations, using ϕ,ψ values that correspond to minima in the χ^2 plots in Fig. 3, are also shown for samples 2 (dashed line, simulated with ϕ,ψ = -62°, 71°) and 3 (dotted line, simulated with ϕ,ψ = -141°, 76°). Details of the measurements are given in the Methods.

Solid-state NMR measurements

Solid-state ^{13}C-NMR measurements were carried out at -125 °C in a 9.39 T field on frozen solutions prepared from nearly equimolar mixtures of 0.5β Fab fragments and ^{13}C-labeled RP135. Samples were prepared with three different doubly ^{13}C-labeled RP135 peptides, labeled at carbonyl sites of Gly 319 and Pro 320, Pro 320 and Gly 321, and Gly 321 and Arg 322 in the GPGR motif (samples 1, 2 and 3, respectively). Examples of one-dimensional ^{13}C magic-angle spinning (MAS) NMR spectra of sample 2 are shown in Fig. 1. In the absence of Fab (Fig. 1*a*), we observe a single carbonyl NMR line at 171.2 p.p.m. with a 6 p.p.m. linewidth typical of structurally heterogeneous peptides in frozen solution. The observed heterogeneity is consistent with liquid-state NMR studies of free V3 peptides[17–22]. In the presence of Fab (Fig. 1*b*), ^{13}C-NMR signals of the labeled peptide are partially obscured by natural-abundance ^{13}C signals of the high-molecular-weight (>50,000 M_r) complex. Double-quantum filtering suppresses these natural-abundance signals and results in a clean spectrum of the labeled carbonyl sites (Fig. 1*c*) with lines 1.5 p.p.m. wide at 168.9 p.p.m. (Gly 321) and at 175.8 p.p.m. (Pro 320). The narrow carbonyl linewidths in the frozen RP135–0.5β Fab complex, which are comparable to those in crystalline peptides[25–27], and the 6.9 p.p.m. chemical-shift difference, which exceeds the random-coil shift difference of ~2.3 p.p.m.[29], provide compelling evidence that the GPGR motif is well structured in the complex in frozen solution.

Two solid-state ^{13}C-NMR methods, developed specifically for investigations of backbone conformations in doubly carbonyl-labeled peptides and proteins[25–28], were applied to samples 1, 2 and 3 to constrain the ϕ and ψ dihedral angles that define the backbone conformation at Pro 320, Gly 321 and Arg 322, respectively. Data from 2D MAS exchange spectroscopy (Fig. 2*a*) take the form of the intensities of crosspeaks that connect MAS sideband lines of the two labeled sites in a 2D spectrum. These intensities depend on the relative orientations of the two carbonyl groups (more precisely, the two carbonyl chemical-shift anisotropy (CSA) tensors), so that the structural information in the data is purely angular in nature, with strong dependences on both ϕ and ψ[25–28]. Data from constant-time double-quantum-filtered dipolar dephasing (CTDQFD) measurements[27] (Fig. 2*b*) take the form of the build-up and decay of carbonyl signal intensity with increasing duration of nuclear spin evolution under an effective magnetic dipole-dipole coupling created by a radiofrequency-driven recoupling (RFDR) pulse sequence[27,30,31]. Because the coupling scales as R^{-3}, where R is the carbon-carbon internuclear distance, CTDQFD curves depend principally on the angle ϕ. Dependence of the effective coupling on the CSA tensor orientations imparts a weaker dependence on ψ (ref. 27). Application of both solid-state NMR methods to the same doubly ^{13}C-labeled samples increases the precision of the structural constraints and minimizes ambiguities that arise from CSA symmetry properties[26] and signal-to-noise limitations. Interference from natural-abundance ^{13}C signals is minimized by double-quantum filtering[27,32] in CTDQFD measurements and by the fact that isolated ^{13}C nuclei contribute only to diagonal and weak intrasite crosspeaks[25,26] in 2D MAS exchange measurements.

Previous experiments on model peptides of known structure[25–28], both in polycrystalline form[25–27] and in noncrystalline frozen solution[27,28], have shown that the 2D MAS exchange and CTDQFD methods employed in this work yield best-fit ϕ and ψ values with an accuracy better than ±10°. The accuracy of related RFDR measurements of internuclear distances has also been convincingly demonstrated on model systems[30].

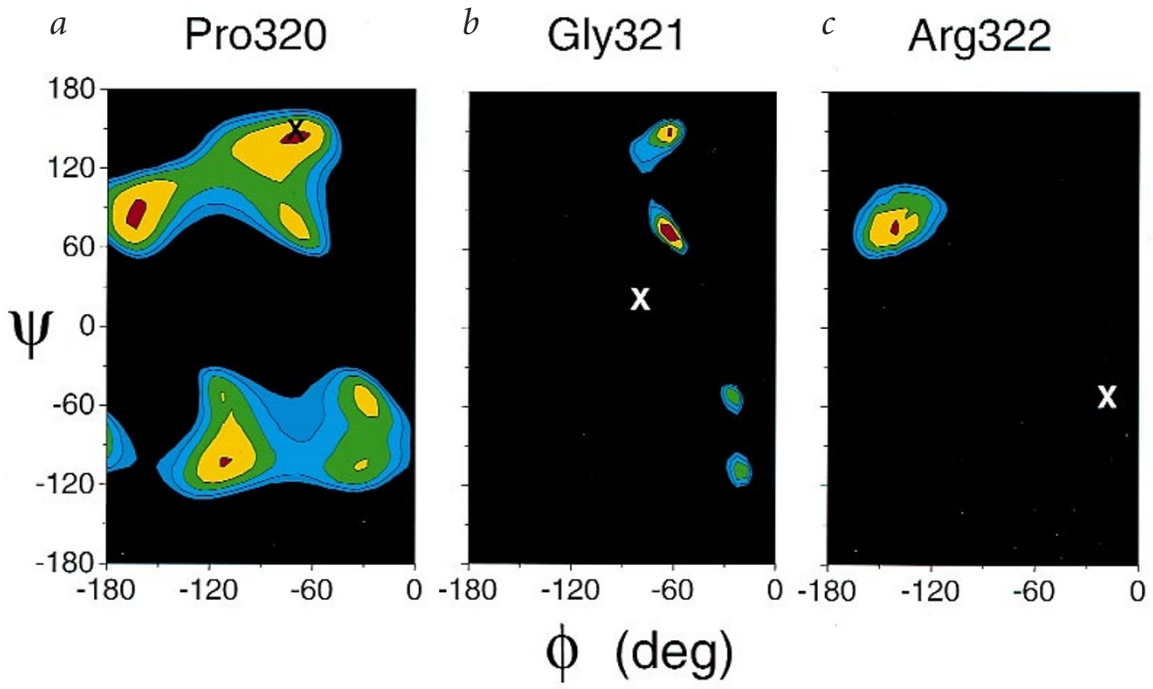

Fig. 3 Total deviation χ^2 between simulated and experimental solid-state NMR data, as a function of the dihedral angles ϕ and ψ assumed in the simulations, for three successive residues in the GPGR motif of the RP135–0.5β Fab complex. Contour levels increase in units of 10, with red regions, which represent the best-fit ϕ and ψ values for each residue, corresponding to $\chi^2 < 21$ (*a*), $\chi^2 < 66$ (*b*) and $\chi^2 < 97$ (*c*). Black regions correspond to $\chi^2 > 61$ (*a*), $\chi^2 > 106$ (*b*) and $\chi^2 > 137$ (*c*). The precision of the solid-state NMR structural constraints is indicated approximately by the sizes of the yellow regions. Crosses indicate ϕ and ψ values for the corresponding residues in the RP142–59.1 Fab complex. These values were extracted from coordinates determined by X-ray crystallography[12], as retrieved from the Protein Data Bank. Cross sizes do not represent uncertainties in the X-ray structure.

Analysis of structural constraints

2D MAS exchange spectra were recorded for all three samples. CTDQFD data were acquired for samples 2 and 3. The data were analyzed by comparison with numerical simulations, as described[25–28]. For each data set, the deviation χ^2 (ϕ,ψ) between experimental and simulated data was evaluated as a function of the ϕ and ψ values assumed in the simulations, with the definition:

$$\chi^2(\phi,\psi) = \frac{1}{\sigma^2}\sum_{i=1}^{N}\{E_i - \lambda(\phi,\psi)\,S_i(\phi,\psi)\}^2 \qquad (1)$$

where E_i and $S_i(\phi,\psi)$ are the experimental and simulated data points, respectively, σ^2 is the mean-squared uncertainty per data point, $\lambda(\phi,\psi)$ is a scaling factor calculated to minimize χ^2 at each ϕ,ψ pair, and N is the number of data points. For samples 2 and 3, the χ^2 values for 2D MAS exchange and CTDQFD data sets were summed to give the total deviation between experiments and simulations. The resulting functions, which display the structural information in the data in an explicit manner, are shown in Fig. 3. Only negative values of ϕ are shown because, for these NMR measurements, $S_i(\phi,\psi) = S_i(-\phi,-\psi)$, so that χ^2 (ϕ,ψ) has inversion symmetry[26]. For Pro 320 (Fig. 3*a*), minima in χ^2 that represent good fits to the NMR data occur at (ϕ,ψ) = (-68°,146°), (-163°,86°) and (-111°,-103°). Of these, only the minimum at (-68°,146°) is physically reasonable because of the well-known restriction of ϕ to the range -70° ± 30° for prolines[33]. For Arg 322 (Fig. 3*c*), a single minimum in χ^2 occurs at (-141°,76°). The symmetry-related minimum at (141°,-76°) is ruled out because this area of the ϕ,ψ plane is not populated by arginines[33]. For Gly 321 (Fig. 3*b*), minima that represent good fits to the data occur at (-62°,71°) and (-62°,151°). The symmetry-related minima at (62°,-71°) and (62°,-151°) also represent allowed glycine conformations.

To determine if any of the four Gly 321 conformations that are consistent with the solid-state NMR data are inconsistent with steric constraints or other energetic considerations, Langevin dynamics (LD) simulations were carried out for the peptide Ac-GPGRA-NH_2 (Gly 319 through Ala 323, with acetyl and amide capping groups) *in vacuo* at 300 K, using the CHARMM simulation program and standard CHARMM bond, angle, improper, van der Waals and electrostatic (but with neutralized arginine side chains) potentials. The χ^2(ϕ,ψ) surfaces for each data set were included in the LD simulations as pseudopotential energies after multiplication by $kT/\sqrt{2(N-1)}$, where the factor of $\sqrt{2(N-1)}$ represents the approximate standard deviation in χ^2 for N - 1 degrees of freedom. The NMR-based pseudopotentials effectively pinned the peptide backbone conformation close to the best-fit ϕ,ψ pairs for Pro 320 and Arg 322 and to any one of the four best-fit ϕ,ψ pairs for Gly 321 listed above, depending on the initial conformation chosen for the simulation run. No significant dependence of the average total CHARMM potential energy on the ϕ,ψ pair adopted by Gly 321 was observed, implying that none of the four Gly 321 conformations can be ruled out on energetic grounds.

Additional constraints on the antibody-bound conformation of RP135 come from liquid-state nuclear Overhauser effect (NOE) data[34], extracted from NOESY difference experiments on RP135–0.5β Fab complexes with selective deuteration, mutation and truncation of the peptide. These constraints define an antiparallel β-sheet structure for residues 311–316 and 324–327 of RP135, which flank the GPGR motif. The GPGR conformation is not constrained by the NOE data[34]. LD simulations on

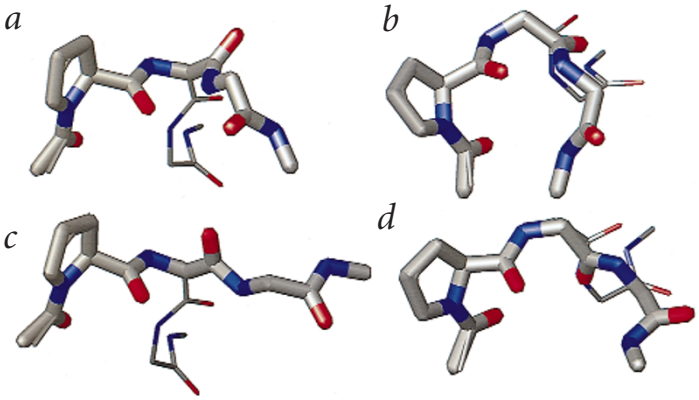

Fig. 4 Backbone conformations for the GPGR motif of the RP135–0.5β complex that are consistent with solid-state NMR data, corresponding to the minima in χ^2 in Fig. 3. Segments shown include C_α of Gly 319 through C_α of Ala 323, which is the portion of the RP135 backbone constrained by the NMR data. Side chains are not shown, with the exception of Pro 320. For comparison, the GPGR backbone conformation in the RP142–59.1 complex[12] is shown in thinner lines. Proline residues in RP135 and RP142 are optimally aligned, and overall orientations are chosen to make clear the conformational differences. ϕ,ψ values for Gly 321 are (*a*) -62°,71°, (*b*) 62°,-71°, (*c*) -62°,151° and (*d*) 62°,-151°. Figure created with the program MOLMOL[44].

residues 311–327 of RP135, incorporating both the solid-state NMR pseudopotentials and 61 interresidue NOE distance constraints, indicate that all four best-fit ϕ,ψ pairs for Gly 321 are consistent with the β-sheet structure proposed[34].

Implications for V3 loop structure and function

Because the monoclonal antibody 0.5β was elicited with intact $gp120_{IIIB}$ (ref. 2), we expect the GPGR conformation in the RP135–0.5β complex to reflect the GPGR conformation in the complex of $gp120_{IIIB}$ with 0.5β. Our NMR data on the RP135–0.5β complex therefore provide atomic-resolution constraints on the structure of a region of gp120 that is of particular biological relevance, in antibody-bound form. As summarized in Table 1, the conformation of the GPGR motif in the RP135–0.5β complex is clearly different from the conformation determined in earlier crystallographic studies of the V3 loop peptide RP142 bound to Fab fragments of monoclonal antibody 59.1[12]. The backbone dihedral angles in the GPGR motif in the RP135–0.5β complex also differ significantly from those of the type II β-turn predicted by sequence analyses[11,13,35] and supported in part by the RP142–59.1[12] and MP1–50.1[12,14] peptide–antibody Fab crystal structures and by liquid-state NMR studies of unbound V3 peptides[16–22]. The GPGR conformation in RP135–0.5β is also different from all other standard β-turns[35]. Although the Pro 320 conformation is similar in all structures in Table 1, all possible ϕ,ψ pairs for Gly 321 and Arg 322 in RP135–0.5β are inconsistent with the type II/type III double β-turn conformation of the GPGR motif in RP142–59.1, as depicted in Fig. 4. The extended conformation of Arg 322 in RP135–0.5β is in marked contrast to the 3_{10}-helix-like conformation in RP142–59.1.

The 59.1 and 0.5β antibodies differ in that the former was elicited with RP70, a 40-residue disulfide-linked V3 loop peptide from HIV-1 strain MN (ref. 3), while the latter was elicited with full-length $gp120_{IIIB}$ (ref. 2). Although both RP135 and RP142 (which represents a central portion of RP70) contain the conserved GPGR motif in their epitopes[2,3], the QR insert immediately preceding GPGR in RP135 is absent in RP142, and the two peptides otherwise differ in 9 of 22 positions. It is therefore not surprising that the GPGR conformations differ in the RP135–0.5β and RP142–59.1 complexes. More specifically, at least three possibilities may account for the difference: (i) the GPGR motif is conformationally heterogeneous in unbound RP70, unbound $gp120_{IIIB}$ or both; (ii) the GPGR conformation is well defined in both unbound RP70 and unbound $gp120_{IIIB}$ but different in the two cases because of sequence differences and the loss of interactions with other regions of gp120 in RP70; (iii) the GPGR conformation is well defined and the same in the unbound states of RP70 and $gp120_{IIIB}$, but is significantly distorted by binding to 59.1, 0.5β or both. The third possibility is at variance with crystallographic studies of other peptide–antibody and protein–antibody complexes[36,37], which generally show little distortion of well-structured protein epitopes upon interaction with antibodies. The second possibility seems unlikely because both 0.5β and 59.1 neutralize the HIV-1 IIIB strain[2,3]. In both cases, neutralization presumably involves binding the GPGR region of $gp120_{IIIB}$, because both 0.5β and 59.1 have been shown to bind the GPGR region of RP135[2,3]. Thus, the GPGR motif in $gp120_{IIIB}$ appears to have sufficient conformational flexibility to adopt both the RP135–0.5β and the RP142–59.1 conformations, in accordance with the first possibility.

There is strong experimental evidence that the V3 loop is a site of interaction between gp120 and the chemokine co-receptors of human T and macrophage cells[5–10] during HIV infection. As in its interactions with neutralizing antibodies, the V3 loop may adopt a well-defined conformation upon interacting with co-receptors. Some viral strains can bind to several distinct co-receptors[6,38,39], an adaptive advantage that may be enhanced by

Table 1 Comparison of backbone dihedral angles (ϕ,ψ) in the GPGR motif of the V3 loop

Residue	RP135–0.5β (solid-state NMR)[1]	RP142–59.1 (crystallography[12])[2]	MP1–50.1 (crystallography[12,14])[2,3]	Standard type II β-turn
Gly 319	nd, nd[4]	98°, -173°	114°, -174°	Undefined
Pro 320	-68°, 146°	-71°, 151°	-77°, 169°	-60°, 120°
Gly 321	±62°, ±71° or ±62°, ±151°	82°, -25°	86°, nd	80°, 0°
Arg 322	-141°, 76°	-19°, -50°	nd, nd	Undefined

[1]Angles for RP135–0.5β are best-fit values.
[2]Angles for RP142–59.1 and MP1–50.1 are determined from coordinates retrieved from the Protein Data Bank.
[3]Angles for MP1–50.1 are averages over two crystallographically inequivalent molecules.
[4]nd = not determined.

the flexibility of the V3 loop. The conserved nature of the GPGR motif may arise out of structural constraints specific to the co-receptor-bound state.

Generality of the methods

The solid-state NMR methods described here are a new general approach to structural investigations of protein-bound peptides, which often serve as useful models for protein–protein interactions. This approach provides local structural constraints that are particularly useful in the testing and development of structural models and when questions of specific structural details are at issue. Crystals are not required. Large (~100,000 M_r) complexes can be studied. The molecular-weight limit is dictated principally by signal-to-noise considerations, not by dynamic correlation times. Association and dissociation rates of the complexes are not important, and binding constants as low as 10^4–10^5 M^{-1} are feasible. Conformations of peptides in complexes with membrane-bound proteins, about which little data are otherwise available, may also be studied with these methods. In contrast to other solid-state NMR methods that provide internuclear distance[40,41] or dihedral-angle[42,43] constraints, the methods described here allow both ϕ and ψ to be determined or constrained by measurements on a single doubly labeled sample.

Methods

Samples for solid-state NMR were prepared by first mixing buffered solutions of labeled peptide and Fab, with typically 0.9 μmol of peptide and 1.0 μmol of Fab in 1 ml of 10 mM phosphate buffer, pH 7.2. Solutions also contained 0.05% NaN_3 as a preservative and 1 mM $CuNa_2EDTA$ to reduce proton spin-lattice relaxation times to roughly 1 s. Sample volumes were reduced to 200 μl by vacuum centrifugation, with care taken to avoid freezing of the sample at this stage. Samples were then pipetted into 6-mm-diameter MAS rotors (240 μl volume), frozen by immersion in liquid nitrogen and then transferred into the precooled MAS NMR probe without thawing.

2D MAS exchange data were obtained with the radiofrequency (rf) pulse sequence CP - t_1 - P - τ - P - t_2, where CP represents cross-polarization from protons to ^{13}C nuclei, t_1 is the evolution period, P is a ^{13}C 90° pulse, τ is the exchange period (500 ms in these measurements) and t_2 is the detection period. Proton decoupling was applied during t_1 and t_2 but not τ. Pulses were synchronized with sample spinning as described[25,26]. Elongated crosspeaks running parallel to the diagonal in Fig. 2*a* are intrasite crosspeaks primarily from natural-abundance ^{13}C nuclei, due to ^{14}N nuclear spin-lattice relaxation[25,26]. CTDQFD data were obtained with the pulse sequence $[CP_y - (RFDR)_L - P_x]_\xi - P_y - (RFDR)_M - P_y - P_x - (RFDR)_N - t_2$ where $(RFDR)_M$ represents application of a rf-driven dipolar recoupling sequence[27,30,31] for M sample rotation periods, x and y indicate rf pulse phases, and ξ represents overall phase shifts for double-quantum filtering[27,32]. In Fig. 2*b*, the total double-quantum-filtered ^{13}C-NMR signal from the labeled carbonyl sites is plotted as a function of the dipolar evolution time, defined as $(M - N)/\nu_R$. M + N is kept constant at 96 for sample 2 and 112 for sample 3. L is 32 for sample 2 and 48 for sample 3. Total acquisition times were ~10 days for each 2D MAS exchange spectrum and ~3 days for each CTDQFD data set. Intensities of intersite crosspeaks between spinning sidebands of order -3 to +3 were measured from 2D MAS exchange spectra for samples 2 and 3, and of order -3 to +2 for sample 1. Intensities of all significant spinning sidebands (order -1 to +1) were summed in CTDQFD spectra.

Simulations of NMR data assumed the CSA tensor orientations and chemical-bond geometries described[26]. For sample 1, 2D MAS exchange simulations were also carried out assuming a *cis* Gly-Pro peptide bond. The global minimum of χ^2 for the *cis* simulations was 19.1, occurring at ϕ,ψ = -70°,150°, so that the possibility of a *cis* Gly-Pro peptide bond in the GPGR motif cannot be ruled out from our data. Carbonyl ^{13}C CSA principal values and resonance assignments were determined from double-quantum-filtered MAS spectra with long double-quantum preparation and mixing periods as follows: (δ_{11}, δ_{22}, δ_{33}) = (242.8, 197.6, 87.0) p.p.m. for Pro 320, (243.0, 171.7, 92.0) p.p.m. for Gly 321, (228.6, 189.2, 94.6) p.p.m. for Arg 322. The principal values (234.9, 179.5, 91.1) p.p.m. for Gly 319 were estimated from MAS spectra of the free peptide. N (number of data points) was 30 for 2D MAS exchange data on sample 1, 42 for 2D MAS exchange data on samples 2 and 3, 6 for CTDQFD data on sample 2, and 7 for CTDQFD data on sample 3. σ^2 is the sum of the mean-squared experimental noise and the estimated mean-squared imprecision of the simulations.

Acknowledgments

This work was supported by a grant to R.T. from the NIH Intramural AIDS Targeted Antiviral Program and by an NIH grant to J.A. We thank S. Matsushita for the hybridoma cell line that produces the 0.5β monoclonal antibody and B.R. Brooks for computational resources.

Correspondence should be addressed to R.T. *email: tycko@helix.nih.gov*

Received 7 July, 1998; accepted 30 October, 1998.

1. Javaherian, K. *et al. Proc. Natl. Acad. Sci. USA* **86**, 6768–6772 (1989).
2. Matsushita, S. *et al. J. Virol.* **62**, 2107–2114 (1988).
3. White-Scharf, M.E. *et al. Virology* **192**, 197–206 (1993).
4. Gorse, G.J., *et al. J. Infect. Dis.* **173**, 330–339 (1996).
5. Freed, E.O., Myers, D.J, & Risser, R. *J. Virol.* **65**, 190–194 (1991).
6. Berger, E.A. *AIDS* **11** (suppl. A), S3–16 (1997).
7. Cocchi, F. *et al. Nature Med.* **2**, 1244–1247 (1996).
8. Wu, L. *et al. Nature* **384**, 179–183 (1996).
9. Trkola, A. *et al. Nature* **384**, 184–187 (1996).
10. Shioda, T., Levy, J.A. & Cheng-Mayer, C. *Proc. Natl. Acad. Sci. USA* **89**, 9434–9438 (1992).
11. LaRosa, G.J. *et al. Science* **249**, 932–935 (1990).
12. Ghiara, J.B., Stura, E.A., Stanfield, R.L., Profy, A.T. & Wilson, I.A. *Science* **264**, 82–85 (1994).
13. Hansen, J.E., Lund, O., Nielse, J.O., Brunak, S. & Hansen, J.-E.S. *Proteins: Struct. Funct. Genet.* **25**, 1–11 (1996).
14. Rini, J.M. *et al. Proc. Natl. Acad. Sci. USA* **90**, 6325–6329 (1993).
15. Ghiara, J.B., Ferguson, D.C., Satterthwait, A.C., Dyson, H.J. & Wilson, I.A. *J. Mol. Biol.* **266**, 31–39 (1997).
16. Jelinek, R. *et al. J. Mol. Biol.* **266**, 649–655 (1997).
17. Chandrasekhar, K., Profy, A.T. & Dyson, H.J. *Biochemistry* **30**, 9187–9194 (1991).
18. Zvi, A., Hiller, R. & Anglister, J. *Biochemistry* **31**, 6972–6979 (1992).
19. Vu, H.M., de Lorimier, R., Moody, M.A., Haynes, B.F. & Spicer, L.D. *Biochemistry* **35**, 5158–5165 (1996).
20. Catasti, P., Bradbury, E.M. & Gupta, G. *J. Biol. Chem.* **271**, 8236–8242 (1996).
21. Vranken, W.F. *et al. Eur. J. Biochem.* **236**, 100–108 (1996).
22. Huang, X., Smith, M.C., Berzofsky, J.A. & Barchi, J.J. *FEBS Lett.* **393**, 280–286 (1996).
23. Kwong, P.D., Wyatt, R., Robinson, J., Sweet, R.W., Sodroski, J. & Hendrickson, W.A. *Nature* **393**, 648–659 (1998).
24. Rusche, J.R. *et al. Proc. Natl. Acad. Sci. USA* **85**, 3198–3202 (1988).
25. Weliky, D.P. & Tycko, R. *J. Am. Chem. Soc.* **118**, 8487–8488 (1996).
26. Tycko, R., Weliky, D.P. & Berger, A.E. *J. Chem. Phys.* **105**, 7915–7930 (1996).
27. Bennett, A.E., Weliky, D.P. & Tycko, R. *J. Am. Chem. Soc.* **120**, 4897–4898 (1998).
28. Long, H.W. & Tycko, R. *J. Am. Chem. Soc.* **120**, 7039–7048 (1998).
29. Richarz, R. & Wuthrich, K. *Biopolymers* **17**, 2133–2141 (1978).
30. Bennett, A.E. *et al. J. Chem. Phys.* **108**, 9463–9479 (1998).
31. Gullion, T. & Vega, S. *Chem. Phys. Lett.* **194**, 423–428 (1992).
32. Tycko, R. & Dabbagh, G. *J. Am. Chem. Soc.* **113**, 9444–9448 (1991).
33. Karplus, P.A. *Prot. Sci.* **5**, 1406–1420 (1996).
34. Zvi, A., Feigelson, D.J., Hayek, Y. & Anglister, J. *Biochemistry* **36**, 8619–8627 (1997).
35. Wilmot, C.M. & Thornton, J.M. *J. Mol. Biol.* **203**, 221–232 (1988).
36. Wilson, I.A. & Stanfield, R.L. *Curr. Opin. Struct. Biol.* **4**, 857–867 (1994).
37. Padlan, E.A., In *Structure of Antigens* (ed. Van Regenmortel, M.H.V.) 29–42 (CRC Press, Boca Raton; Florida;1992).
38. Choe, H. *et al. Cell* **85**, 1135–1148 (1996).
39. Doranz, B.J. *et al. Cell* **85**, 1149–1158 (1996).
40. Gullion, T. & Schaefer, J. *J. Magn. Reson.* **81**, 196–200 (1989).
41. Garbow, J.R. & McWherter, C.A. *J. Am. Chem. Soc.* **115**, 238–244 (1993).
42. Costa, P.R., Gross, J.D., Hong, M. & Griffin, R.G. *Chem. Phys. Lett.* **280**, 95–103 (1997).
43. Feng, X. *et al. J. Am. Chem. Soc.* **119**, 12006–12007 (1997).
44. Koradi, R., Billeter, M. & Wuthrich, K. *J. Mol. Graphics* **14**, 51–55 (1996).